The Arctic winter sea ice quadrupole revisited

Sally Close, M.-N. Houssais, C. Herbaut

The DOI for this manuscript is doi: 10.1175/JCLI-D-16-0506.1

The final published version of this manuscript will replace the preliminary version at the above DOI once it is available.

If you would like to cite this EOR in a separate work, please use the following full citation:

Close, S., M. Houssais, and C. Herbaut, 2017: The Arctic winter sea ice quadrupole revisited. J. Climate. doi:10.1175/JCLI-D-16-0506.1, in press.

The Arctic winter sea ice quadrupole revisited

S. Close*, M.-N. Houssais and C. Herbaut

Sorbonne Universités (UPMC, Univ Paris 06), CNRS-IRD-MNHN, LOCEAN Laboratory, Paris.

**Corresponding author address:* LOCEAN, Université Pierre et Marie Curie, 4 place Jussieu, 75252 Paris Cedex 05, France

E-mail: sally.close@locean-ipsl.upmc.fr

ABSTRACT

The dominant mode of Arctic sea ice variability in winter is often maintained to be represented by a quadrupole structure, comprising poles of one sign in the Okhotsk, Greenland and Barents Seas, and opposing sign in the Labrador and Bering Seas, forced by the North Atlantic Oscillation. In this study, we revisit this large-scale winter mode of sea ice variability using microwave satellite and reanalysis data. We find that the quadrupole structure does not describe a significant covariance relationship amongst all four component poles. The first empirical orthogonal mode, explaining covariability in the sea ice of the Barents, Greenland and Okhotsk Seas, is linked to the Siberian High, whilst the North Atlantic Oscillation exhibits a significant relationship only with the Labrador Sea ice, which varies independently as the second mode. The principal components are characterised by a strong low-frequency signal; the satellite record still being short, statistical analyses should thus be applied cautiously.

1. Introduction

The climate of the Arctic has been reported to have undergone substantial change over recent decades, manifest notably in increasing air temperature (e.g. Serreze et al. 2009) and decreasing sea ice extent (e.g. Maslanik et al. 2007; Comiso et al. 2008), particularly in summer. Whilst the winter sea ice loss has thus far been much less dramatic than that of summer, the changes occurring in this season are nevertheless important, both because of their link to large-scale atmospheric conditions (e.g. Petoukhov and Semenov 2010; Inoue et al. 2012; Screen et al. 2013) and because of their potential role in determining sea ice conditions in the following summer via persistence mechanisms (Day et al. 2014).

The large-scale variability of winter (January-March) sea ice concentration (SIC) has previously been analysed by a number of authors (Walsh and Johnson 1979; Cavalieri and Parkinson 1987; Fang and Wallace 1994; Deser et al. 2000; Ukita et al. 2007, amongst others). Consistent patterns of variability emerge from these studies, suggesting the existence of a "double-dipole", referred to hereafter as a quadrupole, of variability, whereby increases in SIC in the Sea of Okhotsk, Greenland and Barents Seas occur concomitantly with decreases in SIC in the Labrador and Bering Seas (and vice versa). Based on analyses of satellite and atmospheric reanalysis data, a number of studies have hypothesized that the North Atlantic Oscillation (NAO) forces the sea ice mode associated with the quadrupole pattern (Yi et al. 1999; Deser et al. 2000; Ukita et al. 2007), particularly emphasizing the influence on the Atlantic (Barents/Greenland - Labrador) dipole. Such a relationship between Arctic sea ice and the NAO was first proposed prior to the satellite era by Rogers and van Loon (1979), who found a significant link between observation-based indices of sea ice severity in the Baltic Sea and Davis Strait (spanning approximately 90 years) and the NAO. Examining the early winter (October-December) period, Yang and Yuan (2014) suggested that, with recent changes in the large-scale Arctic climate, the "early winter" quadrupole pattern (a pattern that is distinct from that discussed above and in this work, which is formed over the January-March winter season), may have broken down in recent years, primarily due to changes in ice-atmosphere coupling in the Barents Sea region.

In this study, we revisit the large-scale variability of the winter SIC with the aims of ascertaining the robustness of the quadrupole pattern and exploring the hypothesized link with the NAO. Our results demonstrate that the SIC quadrupole pattern does not represent a significant relationship in the covariability of its constituent poles, and that low-frequency variability, which is likely not well resolved by the satellite record at its present length, characterises the form of the associated principal component time series. The influence of the NAO is found to be limited to the Labrador Sea and a small region of the Greenland Sea, and is not well correlated with the dominant mode of sea ice variability. This dominant mode links subregions of the Greenland, Barents and Okhotsk Seas, and appears rather to be predominantly influenced by the Siberian High.

2. Data and Methods

In this work, we analyse SIC using the SMMR-SSM/I-SSMIS data set (for brevity, referred to simply as SSMI hereafter), processed using the bootstrap algorithm (Comiso 2000, updated 2014) and covering the period 1979-2013. As in previous studies, we use empirical orthogonal function (EOF) analysis to describe the large-scale modes of winter SIC. We define the January-March mean SIC field as winter, based on an initial analysis to assess the stability of the modes[1]. The longer-term context is explored using the ECMWF ERA20C reanalysis (Poli et al. 2016), which covers 1900-2010. A preliminary analysis confirms that the data give the same results as the SSMI

[1]Monthly EOF SIC analysis were performed between November and April. The individual monthly January, February and March PC were well correlated amongst themselves and had the same loading pattern; November, December and April, in contrast, yielded weaker correlations and had loading patterns that varied from the other months.

data set over the period common to both (1979-2010). However, the earliest part of the record (prior to 1953) shows negligible variability in an EOF analysis. It seems unlikely that this part of the record is physically realistic, and thus we perform the analysis only on the post-1953 period, over which the variance remains approximately constant. The link with the NAO is investigated using the monthly NAO index supplied by the NOAA Climate Prediction Center (the results are not sensitive to the choice of this index over the equivalent calculated using ERA20C/interim SLP). The significance levels for all correlations are calculated using the effective number of degrees of freedom to account for artificial skill arising from low-frequency variability, following Chelton (1983) (their eq. 1).

3. Results

The loading patterns, percentage of variance explained locally and principal components (PC) for the first EOF mode for the 35 year SSMI record and 58 year ERA20C record are shown in Figure 1. The quadrupole loading pattern emerges as the first mode in both analyses (Figure 1a/c). In both cases, whilst the loading pattern resembles the anticipated quadrupole structure, significant variability is explained only in the Okhotsk and Greenland Seas, and along the coast of Novaya Zemlaya in the Barents Sea (Figure 1b/d). The PC (Figure 1e) are characterised by a decreasing tendency throughout the period. This tendency might equally be viewed as a series of steps, and application of a regime shift algorithm (Rodionov 2004) yields breaks in 1973 (ERA20C only, SSMI begins in 1979), 1983 and 2004 (both ERA20C and SSMI); ANOVA analysis confirms that the means are significantly different over these subperiods. The variability of the Labrador Sea is explained almost entirely by EOF2 (Figure 2), which describes significant variability exclusively in this area (Figure 2b/d). No variability is explained in the Labrador Sea in EOF1, demonstrating that the variability of this region is uncorrelated with that of the other poles of the quadrupole. This can be verified independently of the EOF analysis simply by correlating the sea ice area (SIA) time series of the marginal seas amongst one another (Table 1); the correlations between the SIA of the Labrador Sea and all other regions are low, and in no case significant at either the 90% or 95% level, either in ERA20C or SSMI.

To investigate the link between the quadrupole loading pattern and the NAO found in previous studies (e.g. Deser et al. 2000), the PC are correlated with the DJF mean NAO index (this is the 3-month combination that yields the strongest relationship with JFM SIC in a lagged correlation analysis). The correlation between PC1 and the NAO is low, with $r = 0.29$ ($p = 0.086$) for SSMI, and $r = 0.52$ ($p = 0.104$) for ERA20C. To analyse the spatial extent of the NAO influence on SIC, the winter mean SIC data are regressed on to the index (Figure 3). As for the EOF analysis, the quadrupole loading pattern emerges from the data; however, significant variability is explained only in Baffin Bay, the Labrador Sea and a small region of the Greenland Sea. The Labrador Sea SIA and DJF NAO time series are correlated with $r = 0.48/0.46$ ($p = 0.006/0.003$) for SSMI and ERA20C respectively.

Regression of the DJF SLP on to SIC PC1 does not produce coherent areas of significant correlation for either the ERA20C or SSMI analyses. However, regression of the 700 hPa geopotential height on to SIC PC1 yields a region of significant covariability based over eastern Siberia for both SSMI (Figure 4a) and ERA20C (not shown). Motivated by the proximity of this correlated area to the region forming the basis for the Siberian Index (mean winter normalised 700 hPa geopotential anomalies over 55-70°N, 90-150°E, Overland et al. 2008, shown by the white box in Figure 4a; here, the index is recalculated from ERA20C and over DJF for consistency), the relationship between this metric and SIC PC1 is analysed. SIC PC1 and the Siberian Index (SI) are correlated with $r = 0.62/0.59$ for SSMI / ERA20C respectively ($p = 0.002/0.008$; Figure 4b). The SI time series is filtered with a 2nd order low-pass butterworth filter with a 4-year cutoff frequency to decrease the interannual-scale signal, and the regime shift algorithm used above applied. Breaks are again found in 1973, 1983 and 2004, consistent with the timing of those of SIC PC1 (note that the interannual variability is large relative to the interdecadal signal, and thus no breaks are found in the raw time series, which is dominated by the interannual signal). The SI and SIC PC1 covary most strongly at low-frequencies (>8 yr), although a link is also in evidence at higher frequencies (Figure 5a).

Analysis of subsets of the data reveals that the apparition of the quadrupole loading pattern as the first mode is dependent on the time period chosen for the analysis: if the period 1983-2013 is chosen, removing the sharp decline in the first 4 years of the SSMI record, the quadrupole emerges only as the second PC, and explains significant variability only in the Odden feature of the Greenland Sea (the first mode being the Labrador Sea mode shown in Figure 2). In contrast with previous studies that have suggested the predominance of separate Atlantic and Pacific dipoles, over the full period examined here an East Arctic connection, describing in-phase covariability amongst the Greenland, Barents and Okhotsk Seas, appears rather to be the dominant connection. The Okhotsk and Bering Seas, previously suggested to form a dipole pair in analyses performed over shorter temporal records (Cavalieri and Parkinson 1987; Fang and Wallace 1994), are found not to exhibit significant covariability over the full period of this analysis (Table 1).

SIC PC1 is predominantly characterised by the low-frequency signal: the time series has a decorrelation period of approximately 10 years. Correspondingly, the SIA of the Barents, Greenland and Okhotsk Seas appear to be linked by low-frequency variability: applying the regime shift algorithm of Rodionov (2004) to the SIA time series over the 1979-2013 period, common break points are found (1983 and 2004 in both the Okhotsk and Barents Seas and 2004 in the Greenland Sea). Re-calculating the EOF over the 1983-2004 period (taken as an approximation of a period when the low-frequency variability associated with PC1 is weak), the first and only significant mode is again associated with the quadrupole loading pattern, but now explains significant variability only in the Labrador Sea. SIC PC1 of this reduced period is essentially unaltered compared to the SIC PC2 of the full period ($r = 0.93; p = 0.020$). The low-frequency variability associated with PC2 thus becomes the dominant influence over this subperiod in which the low-frequency variability associated with the original PC1 is weak. No significant covariability amongst the Barents, Greenland and Okhotsk Seas is found over this subperiod, supporting the hypothesis that these regions are linked predominantly by low-frequency variability. Extending this subperiod backwards to 1979, thus corresponding to the 1979-2003 period used in the earlier analysis of Ukita et al. (2007), the same scenario occurs. Here, the quadrupole loading pattern obtained as the first mode again explains significant variability only in the Labrador Sea; consistently, Ukita et al. (2007) noted a significant correlation between this mode and the NAO.

Whilst SIC PC1 is characterised by a strong low-frequency signal, the high-frequency component is also intermittently correlated with the SI (Figure 5a), suggesting that interannual changes in the Greenland, Barents and Okhotsk Seas also experience some influence from the pressure system. In contrast, SIC PC1 is not well correlated in any frequency range with the Arctic Oscillation index ($r = -0.25/-0.40$, $p = 0.15/0.09$ for SSMI and ERA20C respectively), which, as a metric of the large-scale variability, might be expected to better represent the covariability of all three major Arctic pressure centres. This lends support to the idea that it is the gradient at the interface of the Siberian High that is key in determining the sea ice evolution (discussed further below), and that this regional variability is not necessarily well represented by large-scale metrics such as the Arctic Oscillation. This result is consistent with previous studies that have suggested local SLP gradients to control interannual Barents Sea ice variability (Sorteberg and Kvingedal 2006; Schlichtholz and Houssais 2011; Inoue et al. 2012; Herbaut et al. 2015), and with studies that have suggested a combined role of both the Aleutian Low and Siberian High in driving ice-ocean conditions in the Sea of Okhotsk (e.g. Parkinson 1990; Tachibana et al. 1996; Nakanowatari et al. 2014, amongst others).

4. Discussion

The primary modes of winter SIC variability obtained from the above EOF analyses do not describe significant covariability amongst all of the various seas comprising the Northern Hemisphere marginal ice zone (MIZ); rather, subregions of the Greenland, Barents and Okhotsk Seas covary in the first mode and the Labrador Sea varies independently in the second mode. The quadrupole loading pattern itself thus cannot be interpreted to represent a significant relationship amongst its four poles. This can be demonstrated further simply by correlating the SIA calculated over the various seas (Table 1). The only relationship that is significant at the 95% level is that between the Barents and Greenland Sea SIA using ERA20C data. Recent studies have also noted that the co-variability amongst the marginal seas is only weak both at interannual time scales (Chen et al. 2016) and in terms of long-term behaviour (Close et al. 2015) in autumn (November-December), suggesting that this independent regional evolution may not be unique to the winter season examined here.

The link between the strength of the Siberian High and the SIC PC1 inferred here appears physically reasonable given that this feature lies directly adjacent to the Barents and Okhotsk Seas, where PC1 describes variability in the sea ice. Given the length of the available time series, it is not possible to perform a robust physical analysis of the low-frequency signal, which is poorly resolved; we hence focus here on examining the 2004 event, for which the data quality is well known and the step-change in sea ice conditions prolonged and statistically significant (cf. Close et al. 2015). Large-scale changes in the SLP field can be noted before and after 2004, leading to a re-orientation of the isobars over the Barents and Kara Seas (Figure 5b) associated with the expansion of the Siberian High and contraction of the Icelandic Low centre. A statistically significant step-change also occurs in the time series of maximum pressure at the centre of the Siberian High (not shown), corresponding to an increase of $\sim$2 hPa between the 1983-2004 and 2005-2013 mean. As shown in Close et al. (2015), there is a corresponding change in the direction of sea ice export from the Kara Sea before and after this time, with the ice passing predominantly west into the Barents Sea before 2004, but north into the Arctic Ocean afterwards. (At an Arctic-wide scale, the Siberian High was also suggested to trigger changes in the circulation regime of the large-scale sea ice motion in the model-based study of Proshutinsky and Johnson 1997.) Qualitative examination of the pre/post 1973 and 1983 periods (the potential transition dates identified in SIC PC1 by the regime shift algorithm) similarly shows changes either in the strength of the Siberian High itself, or in the adjacent Aleutian or Icelandic Low pressure centres, that translate into a modification of the SLP gradient at the interface with the Siberian High (i.e. over the Okhotsk and Barents Seas respectively). The break points identified statistically here do not correspond to the 1998 cutoff used by Yang and Yuan (2014) for the early winter period; this may suggest a lack of continuity between the autumn/early winter period (Oct-Dec) and the Jan-Mar period analysed here (consistent with their suggestion that the influence of autumn forcing is reduced in the months analysed here and the fact that the atmospheric combination of months that is best correlated with JFM SIC variability here is DJF).

In situ ocean observations remain sparse in the high latitudes, and it has thus not been possible to undertake a direct comparison of the sea ice variability with oceanic heat transport within the context of this study. However, in a model-based analysis, Kawasaki and Hasumi (2016) found that changes in the Siberian High modulated the partitioning of volume transport of the inflowing Atlantic Water between the Fram Strait and Barents Sea Opening. This may implicate a second, consistent mechanism by which the Siberian High could affect the ice cover of the Barents Sea (and thus, partially, the variability associated with PC1) by modulating the volume transport of inflowing warm Atlantic Water, and thus potentially oceanic heat transport to the region. Nevertheless, in contrast with this notion, using an ocean-ice model Herbaut et al. (2015) found that the sudden decline in the SIA of the Barents Sea in 2004 was not preceded by any changes in the inflowing Atlantic Water, and thus suggested that other mechanisms must have been implicated in the sudden ice loss. Herbaut et al. note that ocean heat anomalies that are formed in the Barents Sea Opening take approximately one year to propagate to the ice edge; this suggests that if ocean heat anomalies were forced in phase with changes in the Siberian High at the Barents Sea Opening, any potential impact on the ice edge might be expected to occur at lag. Various authors have also suggested a role of the combined Siberian High - Aleutian Low system in modulating the sea ice cover of the Sea of Okhotsk (e.g. Parkinson 1990; Tachibana et al. 1996). Direct ice advection by the wind (e.g. Kimura and Wakatsuchi 1999; Martin et al. 1998) and oceanic variability (e.g. Nakanowatari et al. 2010) are both generally accepted to play a role in forcing the ice cover in this region, with Nakanowatari et al. (2014) also suggesting the combined Siberian High - Aleutian Low system to have contributed to driving recent oceanic warming in the region.

By definition, the NAO partially describes the variability of the Icelandic Low. The strength of the low can influence the SLP gradient over the Barents Sea, which may suggest an intermittent link between the NAO and PC1 at times when the variability of the Icelandic Low, rather than of the Siberian High, is the dominant control on the SLP gradient over the Barents Sea. An approximation of this gradient is thus defined between the Greenland Sea and northern Russia (shown by the purple boxes in Figure 4a), and found to be well correlated with SIC PC1 ($r = 0.57/0.57$, $p = 0.000/0.012$ for SSMI/ERA20C). The SLP gradient is further found to be correlated with both the SI and NAO ($r = -0.68/-0.56, p = 0.000/0.000$ respectively). Wavelet coherence analysis (Figure 6a) highlights the strong relationship between SIC PC1 and this SLP gradient over a range of frequencies. Further analyses exploring the link with the individual SI and NAO time series (not shown) reveal that the covariance between the SLP gradient and SI strongly resemble the results obtained between SIC PC1 and the SI (Figure 5a); in contrast, the correlation between the SLP gradient and the NAO is limited to low frequencies and to the period 1965-1995. These results support the idea that the SI has exerted an influence on SIC PC1 through its control on the SLP gradient throughout the study period, whilst the influence of the NAO via this same mechanism appears to have been temporally limited to approximately 1965-1995. In early work carried out prior to the satellite era, Rogers and van Loon (1979), employing indices of sea ice severity covering approximately 90 year periods for the Davis Strait and Newfoundland Seas, found covariability between the NAO and Davis Strait sea ice variability, but observed no connection between the NAO and the sea ice of the Barents or East Greenland Seas. The consistency between their results and those obtained here suggests that it might be reasonable to generalise these findings to longer periods.

Whilst there is no overall link between SIC PC1 and the NAO, the two experience common low-frequency variability over the approximate period 1965-1995 (Figure 6b). The link between the NAO and SIC PC1 found by earlier studies (e.g. Walsh and Johnson 1979; Deser et al. 2000) likely arises from this temporally limited connection over an isolated period, rather than representing a continuous influence. In contrast, the link between SIC PC2 and the NAO (again, at low frequencies) is rather consistent, albeit weaker, throughout the study period (Figure 6c). Previous authors have suggested that the link between Arctic sea ice and the NAO is non-stationary (e.g. Smedsrud et al. 2013); however, particularly given the length of the available observational record, the temporally-limited correlation between PC1 and the NAO shown in Figure 6b should also be considered in the context of the cautionary note of Wunsch (1999), where it was emphasized that two uncorrelated stochastic time series may exhibit isolated periods of common low-frequency variability simply by chance. Although, as outlined above, we suggest that the NAO may have played a role in modulating the pressure gradient over the Barents Sea over the 1965-1995 period, the possibility that this correlation (which is based predominantly in the low-frequency range) is fortuitous should thus also be considered. Whilst these factors do not suggest a clear role of the NAO in driving the variability associated with SIC PC1, the consistent correlation between the SI and SIC PC1 found throughout the study period and over multiple frequencies, in contrast, supports the hypothesis of a connection between these two variables.

Both PC1 and PC2 of the winter SIC have a strong low-frequency component. Whilst the two PC are, by definition, uncorrelated over the period of calculation, over certain subperiods (notably 1965-1995), the correlation between the two time series is significant in the low-frequency range (Figure 6d). The dominance of the low-frequency signal, in combination with this evidence that periods of common low-frequency variability can occur in multiple modes (again, cf Wunsch 1999), suggests that long time scales are necessary to achieve separation of the modes. This raises the question of whether, at 35 years, the satellite record is yet long enough to permit robust statistical analysis. Although it is not possible to know whether SIC prior to the advent of the satellite era is realistically reproduced in ERA20C, the modes obtained in this study are consistent between the longer ERA20C period and SSMI.

EOF analyses ultimately provide a statistical, rather than physical, description of the variability of a system and, as noted by numerous authors (e.g. Dommenget and Latif 2002; Monahan et al. 2009), cannot be assumed a priori to represent a physical mode of the system under consideration. The results obtained in the analysis presented here can, however, also be obtained by complementary methods: correlations and wavelet coherence analyses of the SIA of the MIZ support the notion that the individual poles of the quadrupole are, overall, uncorrelated. EOF mode 1 describes covariability amongst only restricted subregions of the Greenland, Barents and Okhotsk poles: regression of the SIC on to the mean SIC calculated along the coast of Novaya Zemlaya confirms the covariability of this region with the significantly correlated subregion of the Sea of Okhotsk that emerges from the EOF analysis. Calculations of the correlations between the SIA of the different MIZ regions and the NAO also support our interpretation that the NAO does not covary significantly with any region outside the Labrador Sea, and regression of the SIC on to the SI confirms that this metric explains significant variability in the Greenland, Barents and Okhotsk Seas. The same results are thus obtained through both the EOF-based and counterpart methods, suggesting that they are not dependent on our choice of analysis method.

5. Conclusions

In summary, we suggest that the quadrupole loading pattern that emerges from EOF analysis of JFM SIC data should not be interpreted physically in and of itself. The loading pattern is found not to be implicitly associated with a particular empirical mode of variability, and should not be assumed to indicate a robust relationship amongst the component poles. This result can be verified by a simple correlation analysis of the SIA of the marginal seas, which shows that the various regions do not covary over the length of the available data record.

EOF1 of both the 1979-2013 sea ice satellite record and the 1953-2010 ERA20C reanalysis represents an East Arctic mode of SIC variability linking restricted sub-regions of the Barents, Greenland and Okhotsk Seas; this contrasts with previous results that found the dominance of an Atlantic dipole of sea ice variability, linking the Barents, Greenland and Labrador Sea. Our analysis suggests that the East Arctic mode is linked to variations in the Siberian High; specifically, we hypothesize that changes in the SLP gradient at the interface between the Siberian High and adjoining Aleutian and Icelandic Low pressure systems modulate the ice cover, either by direct mechanical forcing of the ice cover or indirectly via the ocean (i.e. thermodynamically). These ideas are consistent with existing analyses of regional variability in these regions. The NAO co-varied with PC1 only over a temporally limited period (ca. 1965-1995), but shows more consistent correlation with the Labrador Sea ice cover, which varies independently as EOF2.

Finally, the EOF modes of winter SIC are characterised by low-frequency variability. This is likely not yet well resolved by the satellite record at its present length, highlighting the need for caution when interpreting statistically-based analyses of short records.

Acknowledgments. The research leading to these results has received funding from the European Union 7th Framework Programme (FP7 2007-2013) under grant agreement 308299, NACLIM Project. We are grateful to the reviewers for their helpful comments on the manuscript.

References

Cavalieri, D. J., and C. L. Parkinson, 1987: On the relationship between atmospheric circulation and the fluctuations in the sea ice extents of the Bering and Okhotsk Seas. *J. Geophys. Res.*, **92 (C7)**, 7141–7162, doi:10.1029/JC092iC07p07141.

Chelton, D. B., 1983: Effects of sampling errors in statistical estimation. *Deep Sea Res. A*, **30 (10)**, 1083 – 1103, doi:10.1016/0198-0149(83)90062-6.

Chen, H. W., R. B. Alley, and F. Zhang, 2016: Interannual Arctic sea ice variability and associated winter weather patterns: a regional perspective for 1979–2014. *J. Geophys. Res.*, in press, doi: 10.1002/2016JD024769.

Close, S., M.-N. Houssais, and C. Herbaut, 2015: Regional dependence in the timing of onset of rapid decline in Arctic sea ice concentration. *J. Geophys. Res.*, **120 (12)**, 8077–8098, doi: 10.1002/2015JC011187.

Comiso, J. C., 2000, updated 2014: Bootstrap Sea Ice Concentrations from Nimbus-7 SMMR and DMSP SSM/I-SSMIS. Version 2. doi:10.5067/J6JQLS9EJ5HU.

Comiso, J. C., C. L. Parkinson, R. Gersten, and L. Stock, 2008: Accelerated decline in the Arctic sea ice cover. *Geophys. Res. Lett.*, **35 (1)**, doi:10.1029/2007GL031972.

Day, J. J., S. Tietsche, and E. Hawkins, 2014: Pan-Arctic and Regional Sea Ice Predictability: Initialization Month Dependence. *J. Climate*, **27 (12)**, 4371–4390, doi:10.1175/JCLI-D-13-00614.1.

Deser, C., J. E. Walsh, and M. S. Timlin, 2000: Arctic Sea Ice Variability in the Context of Recent Atmospheric Circulation Trends. *J. Climate*, **13 (3)**, 617–633, doi:10.1175/1520-0442(2000)013⟨0617:ASIVIT⟩2.0.CO;2.

Dommenget, D., and M. Latif, 2002: A Cautionary Note on the Interpretation of EOFs. *J. Climate*, **15 (2)**, 216–225, doi:10.1175/1520-0442(2002)015⟨0216:ACNOTI⟩2.0.CO;2.

Fang, Z., and J. M. Wallace, 1994: Arctic Sea Ice Variability on a Timescale of Weeks and Its Relation to Atmospheric Forcing. *J. Climate*, **7 (12)**, 1897–1914, doi:10.1175/1520-0442(1994)007⟨1897:ASIVOA⟩2.0.CO;2.

Herbaut, C., M.-N. Houssais, S. Close, and A.-C. Blaizot, 2015: Two wind-driven modes of winter sea ice variability in the Barents Sea. *Deep Sea Res. I*, **106**, 97 – 115, doi:10.1016/j.dsr.2015.10.005.

Inoue, J., M. E. Hori, and K. Takaya, 2012: The Role of Barents Sea Ice in the Wintertime Cyclone Track and Emergence of a Warm-Arctic Cold-Siberian Anomaly. *J. Climate*, **25 (7)**, 2561–2568, doi:10.1175/JCLI-D-11-00449.1.

Kawasaki, T., and H. Hasumi, 2016: The inflow of Atlantic water at the Fram Strait and its interannual variability. *J. Geophys. Res.*, **121 (1)**, 502–519, doi:10.1002/2015JC011375.

Kimura, N., and M. Wakatsuchi, 1999: Processes controlling the advance and retreat of sea ice in the Sea of Okhotsk. *J. Geophys. Res.*, **104 (C5)**, 11 137–11 150, doi:10.1029/1999JC900004.

Martin, S., R. Drucker, and K. Yamashita, 1998: The production of ice and dense shelf water in the Okhotsk Sea polynyas. *J. Geophys. Res.*, **103 (C12)**, 27 771–27 782, doi:10.1029/98JC02242.

Maslanik, J., S. Drobot, C. Fowler, W. Emery, and R. Barry, 2007: On the Arctic climate paradox and the continuing role of atmospheric circulation in affecting sea ice conditions. *Geophys. Res. Lett.*, **34 (3)**, L03 711, doi:10.1029/2006GL028269.

Monahan, A. H., J. C. Fyfe, M. H. P. Ambaum, D. B. Stephenson, and G. R. North, 2009: Empirical Orthogonal Functions: The Medium is the Message. *J. Climate*, **22 (24)**, 6501–6514, doi:10.1175/2009JCLI3062.1.

Nakanowatari, T., T. Nakamura, K. Uchimoto, H. Uehara, H. Mitsudera, K. I. Ohshima, H. Hasumi, and M. Wakatsuchi, 2014: Causes of the Multidecadal-Scale Warming of the Intermediate Water in the Okhotsk Sea and Western Subarctic North Pacific. *J. Climate*, **28 (2)**, 714–736, doi: 10.1175/JCLI-D-14-00172.1.

Nakanowatari, T., K. I. Ohshima, and S. Nagai, 2010: What determines the maximum sea ice extent in the Sea of Okhotsk? Importance of ocean thermal condition from the Pacific. *J. Geophys. Res.*, **115 (C12)**, doi:10.1029/2009JC006070, c12031.

Overland, J., S. Rodionov, S. Minobe, and N. Bond, 2008: North Pacific regime shifts: Definitions, issues and recent transitions. *Prog. Oceanogr.*, **77 (2–3)**, 92 – 102, doi:10.1016/j.pocean.2008.03.016.

Parkinson, C. L., 1990: The Impact of the Siberian High and Aleutian Low on the Sea-Ice Cover of the Sea of Okhotsk. *Ann. Glaciol.*, **14 (1)**, 226–229, doi:10.3198/1990AoG14-1-226-229.

Petoukhov, V., and V. A. Semenov, 2010: A link between reduced Barents-Kara sea ice and cold winter extremes over northern continents. *J. Geophys. Res.-Atmos.*, **115 (D21)**, doi:10.1029/2009JD013568, d21111.

Poli, P., and Coauthors, 2016: ERA-20C: An Atmospheric Reanalysis of the Twentieth Century. *J. Climate*, **29 (11)**, 4083–4097, doi:10.1175/JCLI-D-15-0556.1.

Proshutinsky, A. Y., and M. A. Johnson, 1997: Two circulation regimes of the wind-driven Arctic Ocean. *J. Geophys. Res.*, **102 (C6)**, 12 493–12 514, doi:10.1029/97JC00738.

Rodionov, S. N., 2004: A sequential algorithm for testing climate regime shifts. *Geophys. Res. Lett.*, **31 (9)**, doi:10.1029/2004GL019448, l09204.

Rogers, J. C., and H. van Loon, 1979: The Seesaw in Winter Temperatures between Greenland and Northern Europe. Part II: Some Oceanic and Atmospheric Effects in Middle and High Latitudes. *Mon. Wea. Rev.*, **107 (5)**, 509–519, doi:10.1175/1520-0493(1979)107⟨0509:TSIWTB⟩2.0.CO;2.

Schlichtholz, P., and M.-N. Houssais, 2011: Forcing of oceanic heat anomalies by air-sea interactions in the Nordic Seas area. *J. Geophys. Res-Oceans*, **116 (C1)**, doi:10.1029/2009JC005944, c01006.

Screen, J. A., I. Simmonds, C. Deser, and R. Tomas, 2013: The Atmospheric Response to Three Decades of Observed Arctic Sea Ice Loss. *J. Climate*, **26 (4)**, 1230–1248, doi:10.1175/JCLI-D-12-00063.1.

Serreze, M. C., A. P. Barrett, J. C. Stroeve, D. N. Kindig, and M. M. Holland, 2009: The emergence of surface-based Arctic amplification. *The Cryosphere*, **3 (1)**, 11–19, doi:10.5194/tc-3-11-2009.

Smedsrud, L. H., and Coauthors, 2013: The Role of the Barents Sea in the Arctic climate system. *Rev. Geophys.*, **51 (3)**, 415–449, doi:10.1002/rog.20017.

Sorteberg, A., and B. Kvingedal, 2006: Atmospheric Forcing on the Barents Sea Winter Ice Extent. *J. Climate*, **19 (19)**, 4772–4784, doi:10.1175/JCLI3885.1.

Tachibana, Y., M. Honda, and K. Takeuchi, 1996: The abrupt decrease of the sea ice over the southern part of the Sea of Okhotsk in 1989 and its relation to the recent weakening of the Aleutian low. *J. Meteorol. Soc. Jpn.*, **74 (4)**, 579–584.

Ukita, J., M. Honga, H. Nakamura, Y. Tachibana, D. J. Cavalieri, C. L. Parkinson, H. Koide, and K. Yamamoto, 2007: Northern Hemisphere sea ice variability: lag structure and its implications. *Tellus A*, **59 (2)**, 261–272, doi:10.1111/j.1600-0870.2006.00223.x.

Walsh, J. E., and C. M. Johnson, 1979: Interannual atmospheric variability and associated fluctuations in Arctic Sea ice extent. *J. Geophys. Res.*, **84 (C11)**, 6915–6928, doi:10.1029/JC084iC11p06915.

Wunsch, C., 1999: The Interpretation of Short Climate Records, with Comments on the North Atlantic and Southern Oscillations. *Bull. Amer. Meteor. Soc.*, **80 (2)**, 245–255, doi:10.1175/1520-0477(1999)080⟨0245:TIOSCR⟩2.0.CO;2.

Yang, X.-Y., and X. Yuan, 2014: The Early Winter Sea Ice Variability under the Recent Arctic Climate Shift. *J. Climate*, **27 (13)**, 5092–5110, doi:10.1175/JCLI-D-13-00536.1.

Yi, D., L. A. Mysak, and S. A. Venegas, 1999: Decadal-to-interdecadal fluctuations of Arctic sea ice cover and the atmospheric circulation during 1954–1994. *Atmosphere-Ocean*, **37 (4)**, 389–415, doi:10.1080/07055900.1999.9649633.

LIST OF TABLES

	SSMI (1979-2013)							
	Labrador		Greenland		Barents		Okhotsk	
	r	(p)	r	(p)	r	(p)	r	(p)
Greenland	0.04	(0.912)	–	–	–	–	–	–
Barents	-0.02	(0.931)	0.68	(0.090)	–	–	–	–
Okhotsk	0.00	(0.997)	0.51	(0.060)	0.54	(0.130)	–	–
Bering	0.07	(0.722)	-0.41	(0.057)	-0.44	(0.063)	-0.32	(0.180)

	ERA20C (1953-2010)							
	Labrador		Greenland		Barents		Okhotsk	
	r	(p)	r	(p)	r	(p)	r	(p)
Greenland	0.00	(0.995)	–	–	–	–	–	–
Barents	-0.09	(0.640)	**0.65**	**(0.042)**	–	–	–	–
Okhotsk	-0.03	(0.804)	0.53	(0.172)	0.53	(0.139)	–	–
Bering	0.23	(0.270)	-0.20	(0.155)	-0.25	(0.115)	-0.16	(0.251)

TABLE 1. Correlation between JFM mean SIA for regions of MIZ in SSMI and ERA20C. Correlations that are significant at the 95% level are in bold. The regions are defined using the loading patterns resulting from EOF1 (for Okhotsk, Greenland, Barents and Bering) and 2 (for Labrador) obtained using SSMI, corresponding to areas where the magnitude of the loading pattern is greater than 4% within the geographical domains associated with the seas.

LIST OF FIGURES

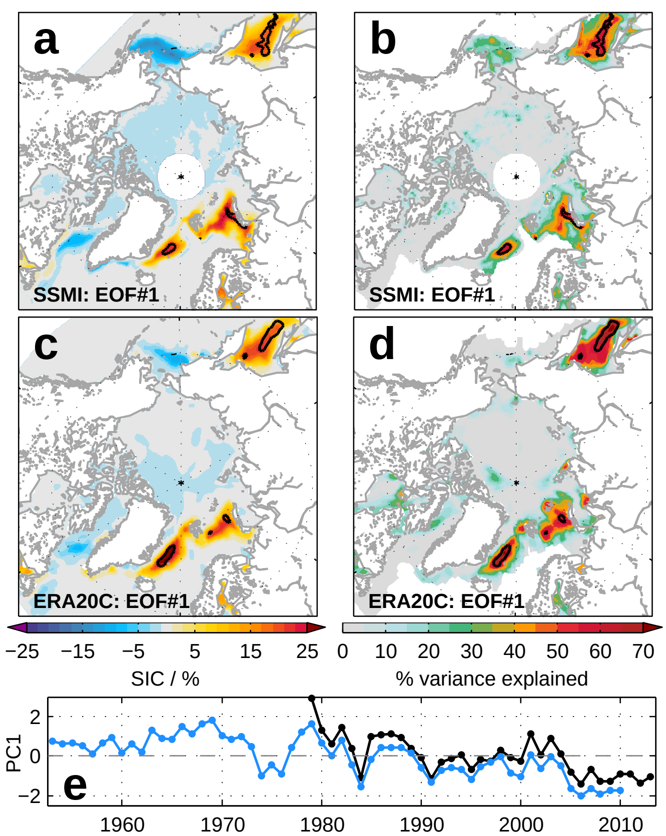

FIG. 1. **(a)** loading pattern and **(b)** percentage of variance explained locally for first EOF mode of winter SIC calculated using SSMI data. **(c/d)** as (a/b) but for ERA20C data. Black contours in a-d indicate the 95% significance level. **(e)** PC mode 1 for SSMI (black) and ERA20C (blue) data.

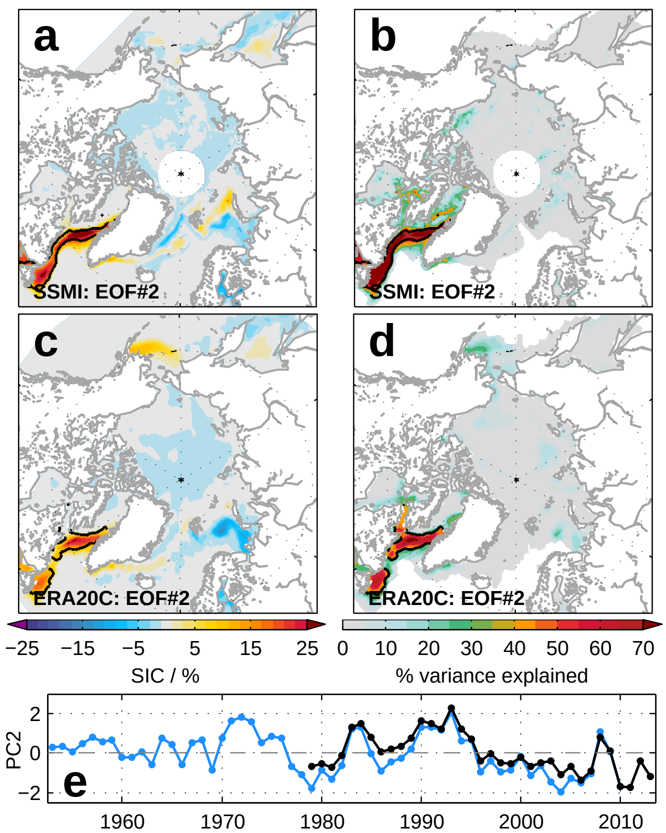

FIG. 2. **(a)** loading pattern and **(b)** percentage of variance explained locally for second EOF mode of winter SIC calculated using SSMI data. **(c/d)** as (a/b) but for ERA20C data. Black contours in a-d indicate the 95% significance level. **(e)** PC mode 2 for SSMI (black) and ERA20C (blue) data.

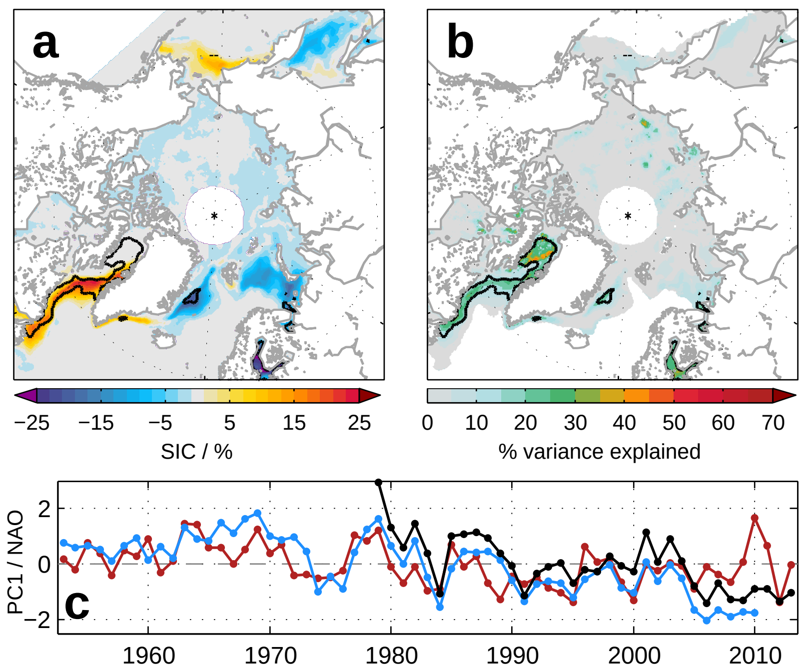

459 FIG. 3. **(a)** regression coefficients and **(b)** percentage of variance explained locally for regression of JFM sea
460 ice on to DJF NAO for SSMI data. Black contours indicate the 95% significance level. **(c)** PC mode 1 for SSMI
461 (black) and ERA20C (blue) data (as for Figure 1) and NAO index (red, sign inverted).

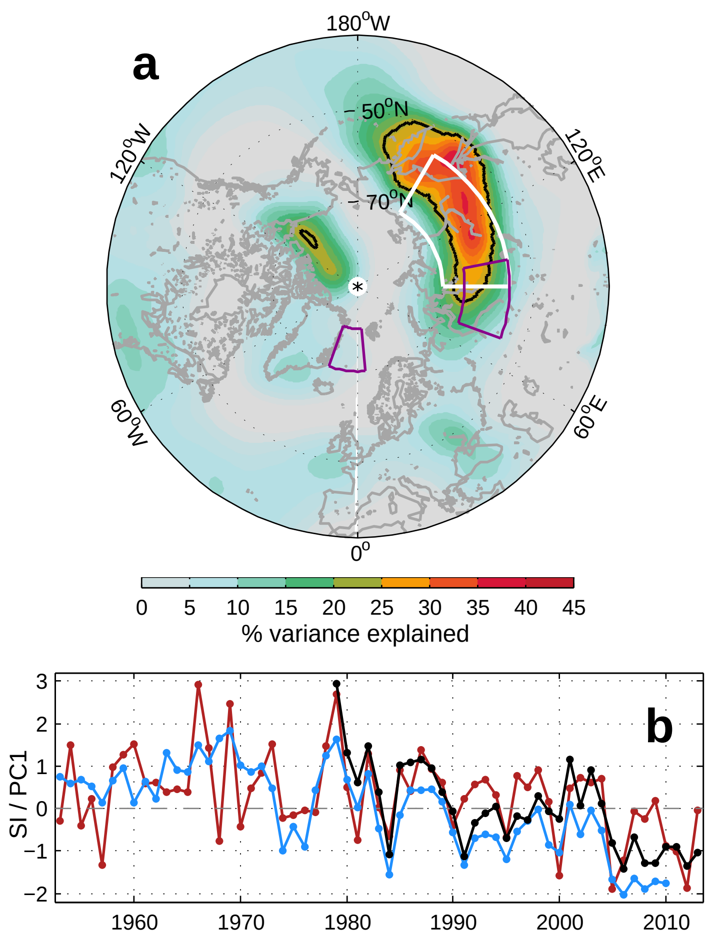

462 FIG. 4. **(a)** percentage of variance explained locally by regression of DJF ϕ_{700} on to SSMI SIC PC1. Black contours show the 95% significance level. White box defines the area over which the Siberian Index is calculated. Purple boxes show the two areas over which the SLP is averaged to estimate the cross-Barents Sea gradient. **(b)** SIC PC mode 1 for SSMI (black) and ERA20C (blue) data (as for Figure 1) and Siberian Index (red, sign inverted for ease of comparison).

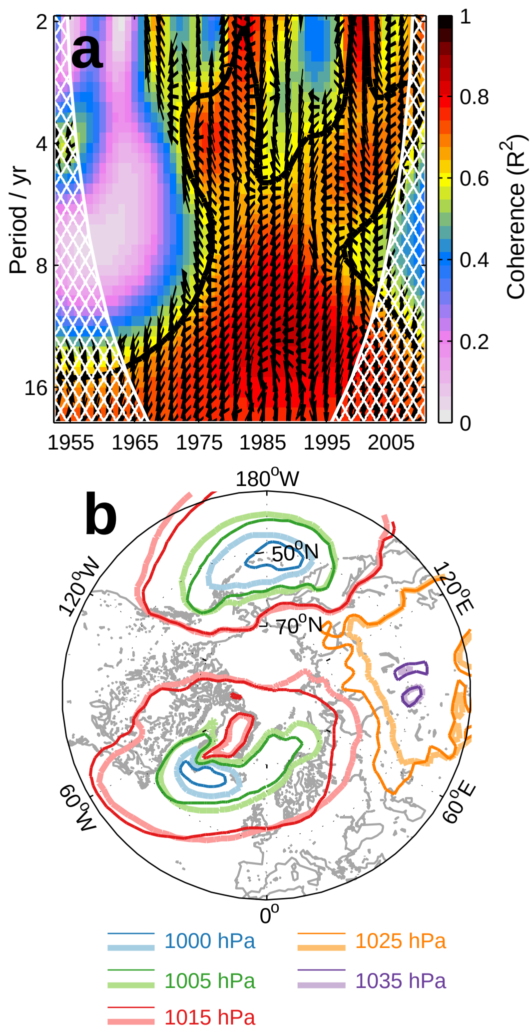

FIG. 5. **(a)** Cross-wavelet coherence between SIC PC1 and Siberian Index. Black contours show the 95% significance level. White hatching denotes results lying outside the cone of influence, where edge artefacts may contaminate the results. Arrows indicate the phase relationship between the two variables, where right/leftwards-pointing arrows indicate that the series are in phase / in anti-phase. **(b)** Mean SLP over 1983-2004 (thick lines, pale colours) and 2005-2010 (thin lines, dark colours); for clarity of comparison, only a limited number of isolines are shown.

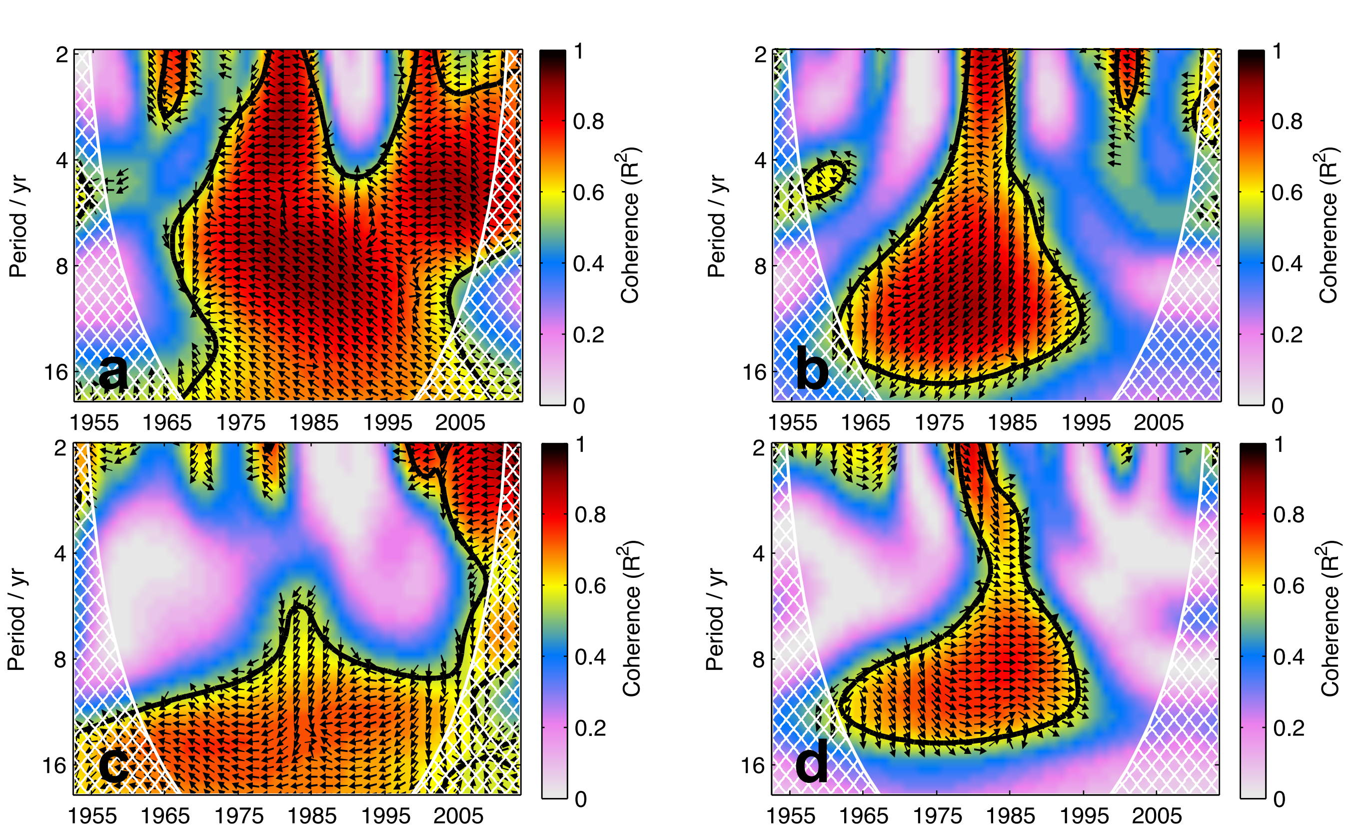

FIG. 6. Cross-wavelet coherence between **(a)** the cross-Barents Sea SLP gradient and SIC PC1; the NAO index and **(b)** SIC PC1 and **(c)** SIC PC2; **(d)** SIC PC1 and SIC PC2. Black contours show the 95% significance level. White hatching denotes results lying outside the cone of influence, where edge artefacts may contaminate the results. Arrows indicate the phase relationship between the two variables as in Figure 5.